

Stability of phantom wormholes

Francisco S. N. Lobo*

*Centro de Astronomia e Astrofísica da Universidade de Lisboa,
Campo Grande, Ed. C8 1749-016 Lisboa, Portugal*

It has recently been shown that traversable wormholes may be supported by phantom energy. In this work phantom wormhole geometries are modelled by matching an interior traversable wormhole solution, governed by the equation of state $p = \omega\rho$ with $\omega < -1$, to an exterior vacuum spacetime at a finite junction interface. The stability analysis of these phantom wormholes to linearized spherically symmetric perturbations about static equilibrium solutions is carried out. A master equation dictating the stability regions is deduced, and by separating the cases of a positive and a negative surface energy density, it is found that the respective stable equilibrium configurations may be increased by strategically varying the wormhole throat radius. The first model considered, in the absence of a thin shell, is that of an asymptotically flat phantom wormhole spacetime. The second model constructed is that of an isotropic pressure phantom wormhole, which is of particular interest, as the notion of phantom energy is that of a spatially homogeneous cosmic fluid, although it may be extended to inhomogeneous spherically symmetric spacetimes.

PACS numbers: 04.20.Gz, 04.20.Jb, 98.80.Es

I. INTRODUCTION

It is now generally accepted that the Universe is undergoing an accelerated phase of expansion [1, 2, 3, 4], where the scale factor obeys $\ddot{a} > 0$. This cosmic acceleration is one of the most challenging current problems in cosmology. Several candidates, responsible for this expansion, have been proposed in the literature, namely, dark energy models, generalizations of the Chaplygin gas, modified gravity and scalar-tensor theories, tachyon scalar fields and braneworld models, amongst others. The dark energy models are parametrized by an equation of state given by $\omega = p/\rho$, where p is the spatially homogeneous pressure and ρ is the dark energy density. For the cosmic expansion, a value of $\omega < -1/3$ is required, as dictated by the Friedman equation $\ddot{a}/a = -4\pi(p+\rho/3)$. A specific exotic form of dark energy, denoted phantom energy, has also been proposed, possessing the peculiar property of $\omega < -1$. This parameter range is not excluded by observation, and possesses peculiar properties, such as the violation of the null energy condition and an infinitely increasing energy density, resulting in a Big Rip, at which point the Universe blows up in a finite time [5]. However, recent fits to supernovae, CMB and weak gravitational lensing data indicate that an evolving equation of state ω crossing the phantom divide -1 , is mildly favored, and several models have been proposed in the literature [6, 7, 8, 9, 10, 11, 12, 13, 14, 15, 16]. In particular, models considering a redshift dependent equation of state, $\omega(z)$, provide significantly ameliorated fits to the most recent and reliable SN Ia supernovae Gold dataset [17].

As the phantom energy equation of state, $p = \omega\rho$ with $\omega < -1$, violates the null energy condition, $p + \rho < 0$, the fundamental ingredient to sustain traversable worm-

hole [18, 19, 20], one now has at hand a possible source for these exotic spacetimes. In fact, this possibility has recently been explored [21, 22], and it was shown that traversable wormholes can be theoretically supported by phantom energy. However, a subtlety needs to be pointed out, as emphasized in Refs. [21, 22]. The notion of phantom energy is that of a homogeneously distributed fluid. When extended to inhomogeneous spherically symmetric spacetimes, the pressure appearing in the equation of state is now a radial pressure, and the transverse pressure is then determined via the field equations. In this context, it is interesting to note that wormhole solutions with an isotropic pressure were found in [22], although these geometries are not asymptotically flat. Sushkov, in Ref. [21], found wormhole geometries by considering specific choices for the distribution of the energy density, and in [22], a complementary approach was traced out, by imposing appropriate choices for the form function and/or the redshift function, and the stress-energy tensor components were consequently determined. In Ref. [22] it was also shown, using the “volume integral quantifier” [23, 24], that these geometries can be theoretically constructed with infinitesimal amounts of averaged null energy condition violating phantom energy.

It is also of a fundamental importance to investigate the stability of these phantom wormhole geometries (It is also interesting to note that a stability analysis of a specific class of traversable wormholes was carried out in Ref. [25], in a rather different context). As in Ref. [22], we shall model these spacetimes by matching an interior traversable wormhole geometry with an exterior Schwarzschild vacuum solution at a junction interface [26, 27, 28, 29]. In this work, we analyze the stability of these phantom wormholes to linearized perturbations around static solutions. Work along these lines was done by considering thin-shell Schwarzschild wormholes, using the cut-and-paste technique [30]. It was later shown that the inclusion of a charge [31] and of a cosmological con-

*Electronic address: flobo@cosmo.fis.fc.ul.pt

stant [32] significantly increases the stable equilibrium configurations found in Ref. [30]. The advantage of this analysis resides in using a parametrization of the stability of equilibrium, so that there is no need to specify a surface equation of state. Note that the stability analysis of these thin-shell wormholes to linearized spherically symmetric perturbations about static equilibrium solutions was carried out by assuming that the shells remain transparent under perturbation [33]. This amounts to considering specific spacetimes that do not contribute with the momentum flux term in the conservation identity, which provides the conservation law for the surface stress-energy tensor. The inclusion of this term, corresponding to the discontinuity of the momentum impinging on the shell, severely complicates the analysis. However, we shall follow the approach of Ishak and Lake [33], with the respective inclusion of the momentum flux term, and deduce a master equation responsible for dictating the stability equilibrium configurations for the specific phantom wormhole geometries found in Ref. [22]. We shall separate the cases of a positive and a negative surface energy density, and find that the stability may be significantly increased by varying the wormhole throat.

This paper is outlined in the following manner. In Section II, we present solutions of a phantom energy traversable wormhole. In Section III, we outline a general linearized stability analysis procedure, and deduce a master equation dictating stable equilibrium configurations. We then apply this analysis to phantom wormhole geometries and determine their respective stability regions. Finally in Section IV, we conclude.

II. PHANTOM ENERGY TRAVERSABLE WORMHOLES

A. Field equations

The interior wormhole spacetime is given by the following metric [18]

$$ds^2 = -e^{2\Phi(r)} dt^2 + \frac{dr^2}{1 - b(r)/r} + r^2 (d\theta^2 + \sin^2 \theta d\phi^2), \quad (1)$$

where $\Phi(r)$ and $b(r)$ are arbitrary functions of the radial coordinate, r , denoted as the redshift function and the form function, respectively [18]. The wormhole throat is located at $b(r_0) = r = r_0$. For the wormhole to be traversable, one must demand that there are no horizons present, which are identified as the surfaces with $e^{2\Phi} \rightarrow 0$, so that $\Phi(r)$ must be finite everywhere. The condition $1 - b/r > 0$ is also imposed. The stress-energy tensor components are given by (with $c = G = 1$)

$$\rho(r) = \frac{1}{8\pi} \frac{b'}{r^2}, \quad (2)$$

$$p_r(r) = \frac{1}{8\pi} \left[-\frac{b}{r^3} + 2 \left(1 - \frac{b}{r} \right) \frac{\Phi'}{r} \right], \quad (3)$$

$$p_t(r) = \frac{1}{8\pi} \left(1 - \frac{b}{r} \right) \left[\Phi'' + (\Phi')^2 - \frac{b'r - b}{2r(r - b)} \Phi' - \frac{b'r - b}{2r^2(r - b)} + \frac{\Phi'}{r} \right], \quad (4)$$

where $\rho(r)$ is the energy density; $p_r(r)$ the radial pressure; and $p_t(r)$ the transverse pressure. The conservation of the stress-energy tensor, $T^{\mu\nu}{}_{;\nu} = 0$, provides us with the following relationship

$$p'_r = \frac{2}{r} (p_t - p_r) - (\rho + p_r) \Phi'. \quad (5)$$

A fundamental ingredient of traversable wormholes and phantom energy is the violation of the null energy condition (NEC), which is defined as $T_{\mu\nu} k^\mu k^\nu \geq 0$, where k^μ is any null vector and the $T_{\mu\nu}$ the stress-energy tensor. Note that for phantom energy, governed by the equation of state $\omega = p/\rho$ with $\omega < -1$, one readily verifies that the NEC is violated, i.e., $p + \rho < 0$. For wormhole spacetimes, consider an orthonormal reference frame with $k^{\hat{\mu}} = (1, \pm 1, 0, 0)$, so that we have

$$T_{\hat{\mu}\hat{\nu}} k^{\hat{\mu}} k^{\hat{\nu}} = \frac{1}{8\pi} \left[\frac{b'r - b}{r^3} + 2 \left(1 - \frac{b}{r} \right) \frac{\Phi'}{r} \right]. \quad (6)$$

Thus, using the flaring out condition of the throat, $(b - b'r)/2b^2 > 0$ [18, 20], and considering the finite character of $\Phi(r)$, we verify that evaluated at the throat the NEC is violated, i.e., $T_{\hat{\mu}\hat{\nu}} k^{\hat{\mu}} k^{\hat{\nu}} < 0$. Matter that violates the NEC is denoted as *exotic matter*.

Note that the notion of phantom energy is that of a homogeneously distributed cosmic fluid. However, as emphasized in [21, 22], it may be extended to inhomogeneous spherically symmetric spacetimes by regarding that the pressure in the equation of state $p = \omega\rho$ is now a radial pressure p_r . The transverse pressure p_t may then be determined from the field equation, in particular, from Eq. (4). Thus, to find phantom energy traversable wormhole spacetimes, we use the equation of state $p_r = \omega\rho$ with $\omega < -1$, representing phantom energy, and thus deduce the following relationship

$$\Phi'(r) = \frac{b + \omega r b'}{2r^2 (1 - b/r)}, \quad (7)$$

by taking into account Eq. (2) and Eq. (3).

To model a traversable wormhole, one now considers appropriate choices for $b(r)$ and/or $\Phi(r)$. Note that this is necessary as we only have four equations, namely, Eqs. (2)-(4), and Eq. (7), with five unknown functions of r , i.e., $\rho(r)$, $p_r(r)$, $p_t(r)$, $b(r)$ and $\Phi(r)$. We shall only consider form functions of the type $b'(r) > 0$, as in cosmology the phantom energy density is considered positive. Now, using the flaring out condition evaluated at the throat [18, 20], we also have the condition $b'(r_0) < 1$.

One may construct asymptotically flat spacetimes, in which $b(r)/r \rightarrow 0$ and $\Phi \rightarrow 0$ as $r \rightarrow \infty$. However, one

may also consider solutions with a cut-off of the stress-energy, by matching the interior solution to an exterior vacuum spacetime, at a junction interface, a . For simplicity, in this paper, we shall consider that the exterior spacetime is the Schwarzschild solution, so that the matching occurs at a junction interface, $r = a$, situated outside the event horizon, i.e., $a > r_b = 2M$, in order to avoid a black hole solution.

B. Specific phantom wormhole models

The physical properties and characteristics of specific phantom energy traversable wormhole models were analyzed in Ref. [22], by considering asymptotically flat spacetimes and by imposing an isotropic pressure. Using the ‘‘volume integral quantifier’’ it was found that it is theoretically possible to construct these geometries with vanishing amounts of averaged null energy condition violating phantom energy. Specific wormhole dimensions and the traversal velocity and time were also deduced from the traversability conditions for a particular wormhole geometry. We shall briefly summarize two specific phantom wormhole models, found in Ref. [22], and for which we shall further analyze the respective stable equilibrium configurations.

Asymptotically flat spacetimes

To construct an asymptotically flat wormhole solution [22], consider $\Phi(r) = \text{const}$. Thus, from Eq. (7) one obtains

$$b(r) = r_0(r/r_0)^{-1/\omega}, \quad (8)$$

so that $b(r)/r = (r_0/r)^{(1+\omega)/\omega} \rightarrow 0$ for $r \rightarrow \infty$. We also verify that $b'(r) = -(1/\omega)(r/r_0)^{-(1+\omega)/\omega}$, so that at the throat the condition $b'(r_0) = 1/|\omega| < 1$ is satisfied.

The stress-energy tensor components are given by

$$p_r(r) = \omega\rho(r) = -\frac{1}{8\pi r_0^2} \left(\frac{r_0}{r}\right)^{3+\frac{1}{\omega}}, \quad (9)$$

$$p_t(r) = \frac{1}{16\pi r_0^2} \left(\frac{1+\omega}{\omega}\right) \left(\frac{r_0}{r}\right)^{3+\frac{1}{\omega}}. \quad (10)$$

Thus, determining the parameter ω from observational cosmology, assuming the existence of phantom energy, one may theoretically construct traversable phantom wormholes by considering the above-mentioned form function and a constant redshift function.

Isotropic pressure, $p_r = p_t = p$

It was found that considering an isotropic pressure, $p_r = p_t = p$, for $\Phi(r)$ to be finite one cannot construct asymptotically flat traversable wormholes [22]. By taking

into account the form function given by $b(r) = r_0(r/r_0)^\alpha$, with $0 < \alpha < 1$, and using Eq. (5) and Eq. (2), one finds that the redshift function is given by

$$\Phi(r) = \left(\frac{3\omega + 1}{1 + \omega}\right) \ln\left(\frac{r}{r_0}\right), \quad (11)$$

where the relationship $\alpha = -1/\omega$ is imposed (see Ref. [22] for details). The stress-energy tensor components are provided by

$$p(r) = \omega\rho(r) = -\frac{1}{8\pi r_0^2} \left(\frac{r_0}{r}\right)^{3+\frac{1}{\omega}}. \quad (12)$$

As noted above, the spacetime is not asymptotically flat. Nevertheless, one may match the interior wormhole solution to an exterior vacuum spacetime at a finite junction surface.

III. STABILITY ANALYSIS

A. Junction conditions

We shall model specific phantom wormholes by matching an interior traversal wormhole geometry, satisfying the equation of state $p_r = \omega\rho$ with $\omega < -1$, with an exterior Schwarzschild solution at a junction interface Σ , situated outside the event horizon, $a > r_b = 2M$.

Using the Darmois-Israel formalism [34, 35], the surface stress-energy tensor, S^i_j , at the junction interface Σ is provided by the Lanczos equations

$$S^i_j = -\frac{1}{8\pi} (\kappa^i_j - \delta^i_j \kappa^k_k), \quad (13)$$

where κ_{ij} is the discontinuity of the extrinsic curvatures across the surface Σ , i.e., $\kappa_{ij} = K^+_{ij} - K^-_{ij}$. The extrinsic curvature is defined as $K_{ij} = n_{\mu;\nu} e^\mu_{(i)} e^\nu_{(j)}$, where n^μ is the unit normal 4-vector to Σ , and $e^\mu_{(i)}$ are the components of the holonomic basis vectors tangent to Σ .

Taking into account the wormhole spacetime metric (1) and the Schwarzschild solution, the non-trivial components of the extrinsic curvature are given by

$$K^{\tau+}_{\tau} = \frac{\frac{M}{a^2} + \ddot{a}}{\sqrt{1 - \frac{2M}{a} + \dot{a}^2}}, \quad (14)$$

$$K^{\tau-}_{\tau} = \frac{\Phi' \left(1 - \frac{b}{a} + \dot{a}^2\right) + \ddot{a} - \frac{\dot{a}^2(b-b'a)}{2a(a-b)}}{\sqrt{1 - \frac{b(a)}{a} + \dot{a}^2}}, \quad (15)$$

and

$$K^{\theta+}_{\theta} = \frac{1}{a} \sqrt{1 - \frac{2M}{a} + \dot{a}^2}, \quad (16)$$

$$K^{\theta-}_{\theta} = \frac{1}{a} \sqrt{1 - \frac{b(a)}{a} + \dot{a}^2}. \quad (17)$$

The Lanczos equation, Eq. (13), then provide us with the following expressions for the surface stresses

$$\sigma = -\frac{1}{4\pi a} \left(\sqrt{1 - \frac{2M}{a} + \dot{a}^2} - \sqrt{1 - \frac{b(a)}{a} + \dot{a}^2} \right) \quad (18)$$

$$\mathcal{P} = \frac{1}{8\pi a} \left[\frac{1 - \frac{M}{a} + \dot{a}^2 + a\ddot{a}}{\sqrt{1 - \frac{2M}{a} + \dot{a}^2}} - \frac{(1 + a\Phi') \left(1 - \frac{b}{a} + \dot{a}^2\right) + a\ddot{a} - \frac{\dot{a}^2(b-b')}{2(a-b)}}{\sqrt{1 - \frac{b(a)}{a} + \dot{a}^2}} \right], \quad (19)$$

where σ and \mathcal{P} are the surface energy density and the tangential surface pressure, respectively.

We shall make use of the conservation identity, which is obtained from the second contracted Gauss-Kodazzi equation or the ‘‘ADM’’ constraint $G_{\mu\nu}e_{(i)}^\mu n^\nu = K_{i|j}^j - K_{,i}$ with the Lanczos equations, and is given by

$$S_{j|i}^i = \left[T_{\mu\nu}e_{(j)}^\mu n^\nu \right]_-^+. \quad (20)$$

The momentum flux term in the right hand side corresponds to the net discontinuity in the momentum which impinges on the shell.

Using $S_{\tau|i}^i = -[\dot{\sigma} + 2\dot{a}(\sigma + \mathcal{P})/a]$, Eq. (20) provides us with

$$\sigma' = -\frac{2}{a}(\sigma + \mathcal{P}) + \Xi, \quad (21)$$

where Ξ , defined for notational convenience, is given by

$$\Xi = -\frac{1}{4\pi a^2} \left[\frac{b'a - b}{2a(1 - \frac{b}{a})} + a\Phi' \right] \sqrt{1 - \frac{b}{a} + \dot{a}^2}. \quad (22)$$

For self-completeness, we shall also include the $\sigma + \mathcal{P}$ term, which is given by

$$\sigma + \mathcal{P} = \frac{1}{8\pi a} \left[\frac{(1 - a\Phi') \left(1 - \frac{b}{a} + \dot{a}^2\right) - a\ddot{a} + \frac{\dot{a}^2(b-b')}{2(a-b)}}{\sqrt{1 - \frac{b(a)}{a} + \dot{a}^2}} - \frac{1 - \frac{3M}{a} + \dot{a}^2 - a\ddot{a}}{\sqrt{1 - \frac{2M}{a} + \dot{a}^2}} \right]. \quad (23)$$

Thus, taking into account Eq. (23), and the definition of Ξ , we verify that Eq. (21) finally takes the form

$$\sigma' = \frac{1}{4\pi a^2} \left(\frac{1 - \frac{3M}{a} + \dot{a}^2 - a\ddot{a}}{\sqrt{1 - \frac{2M}{a} + \dot{a}^2}} - \frac{1 - \frac{3b}{2a} + \frac{b'}{2} + \dot{a}^2 - a\ddot{a}}{\sqrt{1 - \frac{b}{a} + \dot{a}^2}} \right), \quad (24)$$

which, evaluated at a static solution a_0 , shall play a fundamental role in determining the stability regions. Note that Eq. (24) can also be deduced by taking the radial derivative of the surface energy density, Eq. (18).

B. Equation of motion

Rearranging Eq. (18) into the form

$$\sqrt{1 - \frac{2M}{a} + \dot{a}^2} = \sqrt{1 - \frac{b(a)}{a} + \dot{a}^2} - 4\pi\sigma a, \quad (25)$$

we deduce the thin shell’s equation of motion, i.e.,

$$\dot{a}^2 + V(a) = 0, \quad (26)$$

with the potential given by

$$V(a) = 1 + \frac{2M b(a)}{m_s^2} - \left[\frac{m_s}{2a} + \frac{\left(M + \frac{b(a)}{2}\right)}{m_s} \right]^2, \quad (27)$$

where $m_s = 4\pi\sigma a^2$ is the surface mass of the thin shell. However, for computational purposes and notational convenience, we define the following factors

$$F(a) = 1 - \frac{b(a)/2 + M}{a}, \quad (28)$$

$$G(a) = \frac{M - b(a)/2}{a}, \quad (29)$$

so that the potential $V(a)$ takes the form

$$V(a) = F(a) - \left(\frac{m_s}{2a}\right)^2 - \left(\frac{aG}{m_s}\right)^2. \quad (30)$$

Linearizing around a stable solution situated at a_0 , we consider a Taylor expansion of $V(a)$ around a_0 to second order, given by

$$V(a) = V(a_0) + V'(a_0)(a - a_0) + \frac{1}{2}V''(a_0)(a - a_0)^2 + O[(a - a_0)^3]. \quad (31)$$

The first and second derivatives of $V(a)$ are given by

$$V'(a) = F' - 2\left(\frac{m_s}{2a}\right)\left(\frac{m_s}{2a}\right)' - 2\left(\frac{aG}{m_s}\right)\left(\frac{aG}{m_s}\right)' \quad (32)$$

$$V''(a) = F'' - 2\left[\left(\frac{m_s}{2a}\right)'\right]^2 - 2\left(\frac{m_s}{2a}\right)\left(\frac{m_s}{2a}\right)'' - 2\left[\left(\frac{aG}{m_s}\right)'\right]^2 - 2\left(\frac{aG}{m_s}\right)\left(\frac{aG}{m_s}\right)'' \quad (33)$$

respectively. Evaluated at the static solution, at $a = a_0$, we verify that $V(a_0) = 0$ and $V'(a_0) = 0$. From the condition $V'(a_0) = 0$, one extracts the following useful equilibrium relationship

$$\Gamma \equiv \left(\frac{m_s}{2a_0}\right)' = \left(\frac{a_0}{m_s}\right) \left[F' - 2\left(\frac{a_0 G}{m_s}\right)\left(\frac{a_0 G}{m_s}\right)' \right], \quad (34)$$

which will be used in determining the master equation, responsible for dictating the stable equilibrium configurations.

The solution is stable if and only if $V(a)$ has a local minimum at a_0 and $V''(a_0) > 0$ is verified. The latter condition takes the form

$$\left(\frac{m_s}{2a}\right) \left(\frac{m_s}{2a}\right)'' < \Psi - \Gamma^2, \quad (35)$$

where Ψ is defined as

$$\Psi = \frac{F''}{2} - \left[\left(\frac{aG}{m_s} \right)' \right]^2 - \left(\frac{aG}{m_s} \right) \left(\frac{aG}{m_s} \right)'' . \quad (36)$$

C. The master equation

Using $m_s = 4\pi a^2 \sigma$, and taking into account the radial derivative of σ' , Eq. (21) can be rearranged to provide the following relationship

$$\left(\frac{m_s}{2a}\right)'' = \Upsilon - 4\pi\sigma'\eta, \quad (37)$$

with the parameter η defined as $\eta = \mathcal{P}'/\sigma'$, and Υ given by

$$\Upsilon \equiv \frac{4\pi}{a} (\sigma + \mathcal{P}) + 2\pi a \Xi'. \quad (38)$$

Equation (37) will play a fundamental role in determining the stability regions of the respective solutions. Note that the parameter $\sqrt{\eta}$ is normally interpreted as the speed of sound, so that one would expect that $0 < \eta \leq 1$, based on the requirement that the speed of sound should not exceed the speed of light. However, in the presence of exotic matter this cannot naively be done so. Therefore, in this work the above range will be relaxed. We refer the reader to Ref. [30] for an extensive discussion on the respective physical interpretation of η in the presence of exotic matter.

We shall use η as a parametrization of the stable equilibrium, so that there is no need to specify a surface equation of state. Thus, substituting Eq. (37) into Eq. (35), one deduces the master equation given by

$$\sigma' m_s \eta_0 > \Theta, \quad (39)$$

where $\eta_0 = \eta(a_0)$ and Θ is defined as

$$\Theta \equiv \frac{a_0}{2\pi} (\Gamma^2 - \Psi) + \frac{1}{4\pi} m_s \Upsilon. \quad (40)$$

Now, from the master equation we find that the stable equilibrium regions are dictated by the following inequalities

$$\eta_0 > \bar{\Theta}, \quad \text{if } \sigma' m_s > 0, \quad (41)$$

$$\eta_0 < \bar{\Theta}, \quad \text{if } \sigma' m_s < 0, \quad (42)$$

with the definition

$$\bar{\Theta} \equiv \frac{\Theta}{\sigma' m_s}. \quad (43)$$

We shall now model the phantom wormhole geometries by choosing the specific form and redshift functions considered in Ref. [22], and consequently determine the stability regions dictated by the inequalities (41)-(42). In the specific cases that follow, the explicit form of $\bar{\Theta}$ is extremely messy, so that as in [33], we find it more instructive to show the stability regions graphically.

D. Stability regions

Asymptotically flat spacetimes

Consider the specific choices for the redshift and form functions given by

$$\Phi(r) = \text{const}, \quad (44)$$

$$b(r) = r_0(r/r_0)^{-1/\omega}, \quad (45)$$

respectively. These are solutions to Eq. (7), for an asymptotically flat spacetime.

The factor related to the net discontinuity of the momentum flux impinging on the shell, Ξ , is provided by

$$\Xi = \frac{1}{8\pi a_0^2} \frac{\left(\frac{1+\omega}{\omega}\right) \left(\frac{r_0}{a_0}\right)^{\frac{1+\omega}{\omega}}}{\sqrt{1 - \left(\frac{r_0}{a_0}\right)^{\frac{1+\omega}{\omega}}}}. \quad (46)$$

The factor deduced from the equilibrium condition, Γ , is given by

$$\Gamma = \frac{1}{2a_0} \left[\frac{1}{2} \frac{\left(\frac{1+\omega}{\omega}\right) \left(\frac{r_0}{a_0}\right)^{\frac{1+\omega}{\omega}}}{\sqrt{1 - \left(\frac{r_0}{a_0}\right)^{\frac{1+\omega}{\omega}}}} - \frac{\frac{M}{a_0}}{\sqrt{1 - \frac{2M}{a_0}}} \right]. \quad (47)$$

The radial derivative of the surface energy density, σ' , evaluated at the static solution, which will be fundamental in determining the stability regions, takes the following form

$$\sigma' = \frac{1}{4\pi a_0^2} \left(\frac{1 - \frac{3M}{a_0}}{\sqrt{1 - \frac{2M}{a_0}}} - \frac{1 - \left(\frac{1+\omega}{2\omega}\right) \left(\frac{r_0}{a_0}\right)^{\frac{1+\omega}{\omega}}}{\sqrt{1 - \left(\frac{r_0}{a_0}\right)^{\frac{1+\omega}{\omega}}}} \right). \quad (48)$$

We shall not write down the explicit forms of the remaining functions, i.e., Υ , Ψ and Θ , as they are extremely lengthy. However, the stability regions shall be shown graphically.

To determine the stability regions of this solution, we shall separate the cases of $b(a_0) < 2M$ and $b(a_0) > 2M$. From Eq. (18) and the definition of $m_s = 4\pi a_0^2 \sigma$, this corresponds to $m_s > 0$ and $m_s < 0$, respectively. Here, we shall relax the condition that the surface energy density be positive, as in considering traversable wormhole

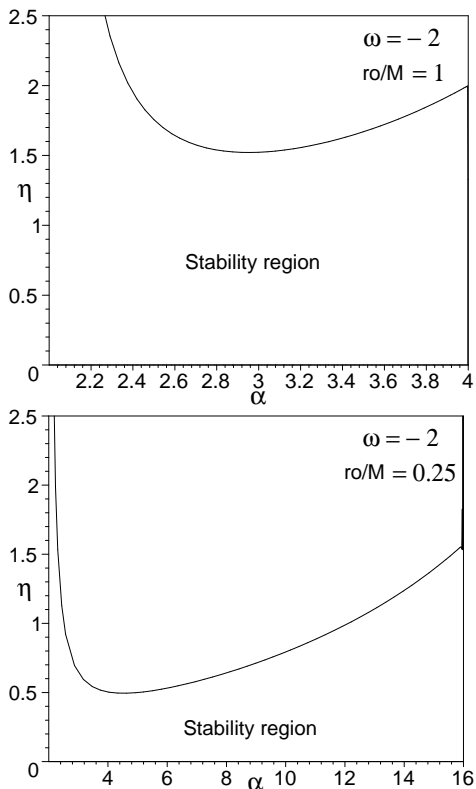


FIG. 1: Plots for a positive surface energy density, i.e., $b(a_0) < 2M$. We have defined $\alpha = a_0/M$, and considered $\omega = -2$ for both cases. The first plot is given by $r_0/M = 1$, and the second by $r_0/M = 0.25$. The stability regions are given below the solid curve. See the text for details.

geometries, one is already dealing with exotic matter. Note that for $\sigma < 0$, the weak energy condition is readily violated.

For $b(a_0) < 2M$, i.e., for a positive surface energy density, and using the form function, Eq. (45), we need to impose the condition $r_0 < 2M$, so that the junction radius lies outside the event horizon, $a_0 > 2M$. Thus, the junction radius lies in the following range

$$2M < a_0 < 2M \left(\frac{2M}{r_0} \right)^{-(1+\omega)}. \quad (49)$$

For a fixed value of ω , we verify that as $r_0 \rightarrow 0$, then $a_0 \rightarrow \infty$. The range decreases, i.e., $a_0 \rightarrow 2M$, as $r_0 \rightarrow 2M$. Note that by fixing r_0 and decreasing ω , the range of a_0 is also significantly increased.

For a fixed value of the parameter, for instance $\omega = -2$, we shall consider the following cases: $r_0/M = 1.0$, so that $2 < a_0/M < 4$; and for $r_0/M = 0.25$, we have $2 < a_0/M < 16$. The respective stability regions are depicted in Fig. 1. From Eq. (48) we find that $\sigma' < 0$, and as we are considering a positive surface energy density, this implies $m_s \sigma' < 0$. Thus, the stability regions, dictated by the inequality (42), lie beneath the solid lines in the plots of Fig. 1. Note that for decreasing values of r_0/M , despite the fact that the range of a_0 increases,

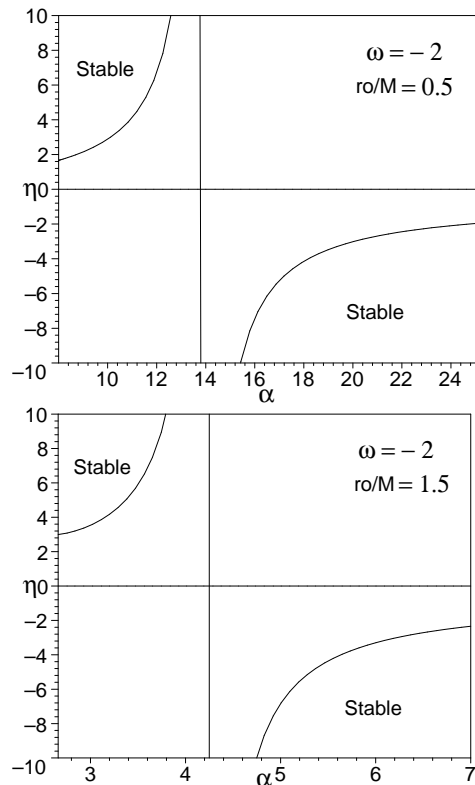


FIG. 2: Plots for a negative surface energy density, considering $r_0/M < 2$. We have defined $\alpha = a_0/M$, and considered $\omega = -2$ for both cases. The first plot is given by $r_0/M = 0.5$, and the second by $r_0/M = 1.5$. The stability regions are given above the first solid curve, and below the second solid curve. See the text for details.

the values of η_0 are further restricted. Thus, adopting a conservative point of view, using positive surface energy densities, we note that stable phantom wormhole geometries may be found well within the bound of $0 < \eta_0 \leq 1$, and the stability regions increase for increasing values of r_0/M .

For $b(a_0) > 2M$, the surface mass of the thin shell is negative, $m_s(a_0) < 0$. We shall separate the cases of $r_0 < 2M$ and $r_0 > 2M$.

If $r_0 < 2M$, the range of the junction radius is given by

$$a_0 > 2M \left(\frac{2M}{r_0} \right)^{-(1+\omega)}. \quad (50)$$

For this specific case, σ' possesses one real positive root, R , in the range of Eq. (50), signalling the presence of an asymptote, $\sigma'|_R = 0$. We verify that $\sigma' < 0$ for $2M(2M/r_0)^{-(1+\omega)} < a_0 < R$, and $\sigma' > 0$ for $a_0 > R$. Thus, the stability regions are given by

$$\eta_0 > \bar{\Theta}, \quad \text{if } 2M \left(\frac{2M}{r_0} \right)^{-(1+\omega)} < a_0 < R, \quad (51)$$

$$\eta_0 < \bar{\Theta}, \quad \text{if } a_0 > R. \quad (52)$$

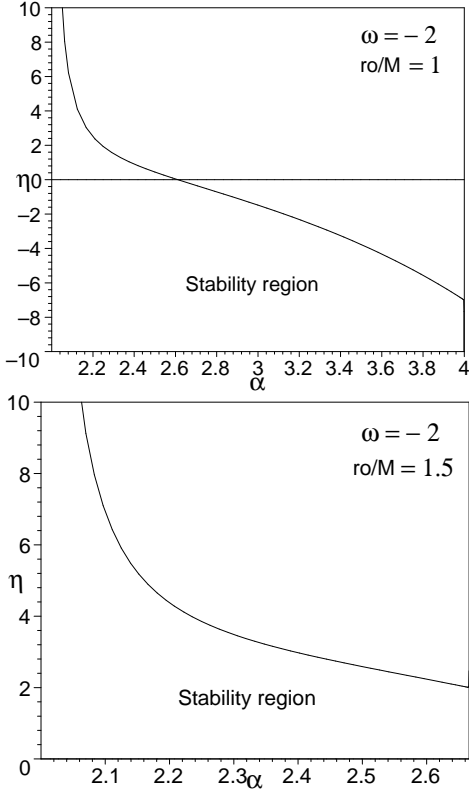


FIG. 3: Plots for an isotropic pressure phantom wormhole. We have defined $\alpha = a_0/M$ and considered $\omega = -2$ for both cases. For $b(a_0) < 2M$, the condition $r_0 < 2M$ is imposed. The first plot is given by $r_0/M = 1.0$, and the second by $r_0/M = 1.5$. The stability regions are given below the solid curves.

Consider for $\omega = -2$, the particular cases of $r_0/M = 0.5$, so that $a_0/M > 8$, and $r_0/M = 1.5$, so that $a_0/M > 2.667$. The asymptotes, $\sigma'|_R = 0$, for these cases exist at $R/M \simeq 13.9$ and $R/M \simeq 4.24$, respectively. These cases are represented in Fig. 2. Note that for increasing values of r_0/M , the range of a_0 decreases, and the values of η_0 are less restricted. Thus, one may conclude that the stability regions increase, for increasing values of r_0/M .

If $r_0 > 2M$, then obviously $a_0 > r_0$. We verify that $\sigma' > 0$, and consequently $m_s \sigma' < 0$, so that the stability region is given by inequality (42). We verify that the values of η_0 are always negative. However, by increasing r_0/M , the values of η_0 become less restricted, and the range of a_0 decreases.

Isotropic pressure, $p_r = p_t = p$

Consider the following functions

$$\Phi(r) = \left(\frac{3\omega + 1}{1 + \omega} \right) \ln(r/r_0), \quad (53)$$

$$b(r) = r_0 (r/r_0)^{-1/\omega}, \quad (54)$$

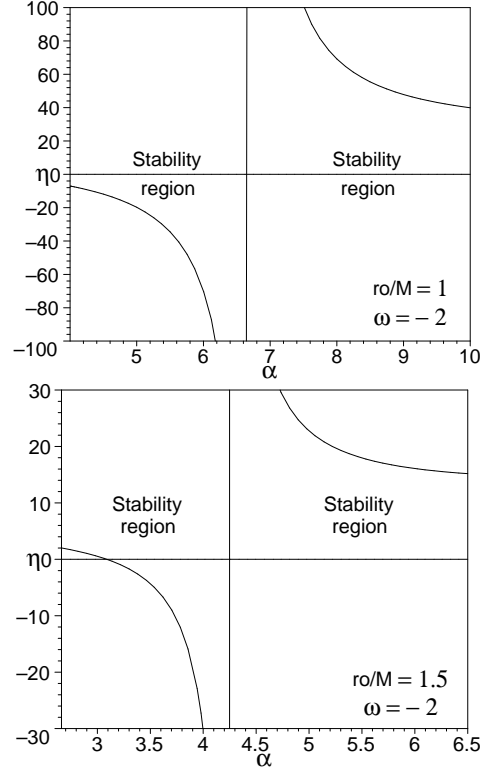


FIG. 4: Plots for an isotropic pressure phantom wormhole, for $b(a_0) > 2M$ and $r_0 < 2M$. We have defined $\alpha = a_0/M$ and considered $\omega = -2$ for both cases. The first plot is given by $r_0/M = 1.0$, and the second by $r_0/M = 1.5$. The stability regions are given above the first solid curve, and below the second solid curve.

which are solutions of a phantom wormhole possessing an isotropic pressure [22].

The factor related to the momentum flux term, Ξ , is given by

$$\Xi = \frac{1}{8\pi a_0^2} \sqrt{1 - \left(\frac{r_0}{a_0} \right)^{\frac{1+\omega}{\omega}}} \left[\frac{\left(\frac{1+\omega}{\omega} \right) \left(\frac{r_0}{a_0} \right)^{\frac{1+\omega}{\omega}}}{1 - \left(\frac{r_0}{a_0} \right)^{\frac{1+\omega}{\omega}}} - \frac{6\omega}{1 + \omega} \right]. \quad (55)$$

The Γ and σ' are identical to the previous case of an asymptotically flat spacetime, and as before we shall not show the specific forms of the remaining functions, as they are extremely lengthy.

To determine the stability regions of this solution, as in the previous case, we shall separate the cases of $b(a_0) < 2M$ and $b(a_0) > 2M$.

For $b(a_0) < 2M$, we have $m_s > 0$, and the condition $r_0 < 2M$ is imposed. Therefore, the junction radius lies in the same range as the previous case, i.e., Eq. (49). We also verify that $\sigma' < 0$ in the respective range. Thus the stability region is given by

$$\eta_0 < \bar{\Theta}, \quad \text{if } 2M < a_0 < 2M \left(\frac{2M}{r_0} \right)^{-(1+\omega)}. \quad (56)$$

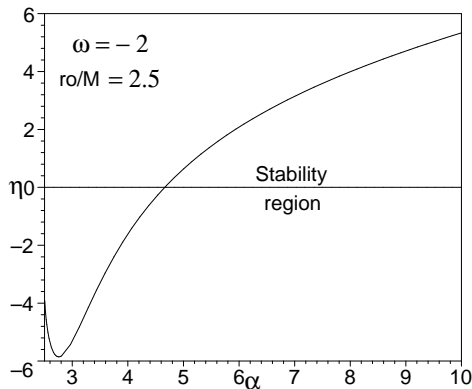


FIG. 5: Plot for an isotropic pressure phantom wormhole, considering a negative surface energy density, with $r_0/M = 2.5$. We have defined $\alpha = a_0/M$ and considered $\omega = -2$. The stability region is given below the solid curve. See the text for details.

Consider, for simplicity, $\omega = -2$, and the cases for $r_0/M = 1$ and $r_0/M = 1.5$ are analyzed in Fig. 3. The ranges are given by $2 < a_0/M < 4$ and $2 < a_0/M < 2.667$, respectively. Note that as r_0/M decreases, the range of a_0 increases. However, the values of the parameter η_0 become more restricted. Thus, one may conclude that the stability regions increase, as r_0/M increases.

For $b(a_0) > 2M$, then $m_s(a_0) < 0$. As before, we shall separate the cases of $r_0 < 2M$ and $r_0 > 2M$. For $r_0 < 2M$, the range of a_0 is given by $a_0 > 2M(2M/r_0)^{-(1+\omega)}$, as in the previous case of the asymptotically flat wormhole spacetime.

For this case σ' also possesses one real positive root, R , in the respective range. We have $\sigma' < 0$ for $(2M/r_0)^{-1/\omega} < a < R$, and $\sigma' > 0$ for $a_0 > R$. The stability regions are also given by the conditions (51)-(52). We have considered the specific cases of $r_0/M = 1$ so that the respective range is $a_0/M > 4$; and $r_0/M = 1.5$, so that $a_0/M > 2.667$. The asymptotes, $\sigma'|_R = 0$, for these cases exist at $R/M \simeq 6.72$ and $R/M \simeq 4.24$, respectively. This analysis is depicted in the plots of Fig. 4. Note that the plots given by Θ are inverted relatively to the asymptotically flat spacetime. For decreasing values of r_0/M , note that the value of the stability parameter η_0 becomes less restricted and the range of the junction radius increases. Thus, one may conclude that the stability regions increase for decreasing values of r_0/M .

If $r_0 > 2M$, then $a_0 > r_0$. We find that $\sigma' > 0$, which implies $m_s\sigma' < 0$. Consider $\omega = -2$, and the specific case of $r_0/M = 2.5$, so that the stability region lies below the solid line in Fig. 5. We also verify that for increasing values of r_0/M , the values of the parameter η_0 become further restricted. Thus, one may conclude that the stability regions decrease for increasing values of r_0/M .

IV. SUMMARY AND DISCUSSION

As the Universe is probably constituted of approximately 70% of null energy condition violating phantom energy, this cosmic fluid may be used as a possible source to theoretically construct traversable wormholes. In fact, it was found that infinitesimal amounts of phantom energy may support traversable wormholes [22]. In this paper, we have modelled phantom wormholes by matching an interior traversable wormhole geometry, satisfying the equation of state $p = \omega\rho$ with $\omega < -1$, to an exterior vacuum solution at a finite junction interface. We have analyzed the stability of these phantom wormholes, an issue of fundamental importance, to linearized perturbations around static solutions, by including the momentum flux term in the conservation identity. We have considered two particularly interesting cases, namely, that of an asymptotically flat spacetime, and that of an isotropic pressure wormhole geometry. The latter solution is of particular interest, as the notion of phantom energy is that of a spatially homogeneous cosmic fluid, although it may be extended to inhomogeneous spherically symmetric spacetimes. We have separated the cases of positive and negative surface energy densities and found that the stable equilibrium regions may be significantly increased by strategically varying the wormhole throat. As we are considering exotic matter, we have relaxed the condition $0 < \eta_0 \leq 1$, and found stability regions for phantom wormholes well beyond this range. There are several known examples of exotic $\eta_0 < 0$ behavior, namely the Casimir effect and the false vacuum [30], so that one cannot *a priori* impose $0 < \eta_0 \leq 1$ until a detailed microphysical model of exotic matter is devised.

As emphasized in Ref. [22], these stable phantom wormholes have far-reaching physical and cosmological implications. First, apart from being used for interstellar travel, they may be transformed into time-machines [19, 20], consequently violating causality with the associated time travel paradoxes. Relative to the cosmological consequences, the existence of phantom energy presents us with a natural scenario for traversal wormholes. It was shown by González-Díaz [36], that due to the fact of the accelerated expansion of the Universe, macroscopic wormholes could naturally be grown from the quantum foam. It was shown that the wormhole's size increases by a factor which is proportional to the scale factor of the Universe, and still increases significantly if the cosmic expansion is driven by phantom energy [37]. However, it was also found that using wormholes modelled by thin shells accreting phantom energy [38], the wormholes become asymptotically comoving with the cosmological background as the Big Rip is approached, so that the future of the universe is shown to be causal.

-
- [1] A. Grant *et al*, “The Farthest known supernova: Support for an accelerating Universe and a glimpse of the epoch of deceleration,” *Astrophys. J.* **560** 49-71 (2001) [arXiv:astro-ph/0104455].
- [2] S. Perlmutter, M. S. Turner and M. White, “Constraining dark energy with SNe Ia and large-scale structure,” *Phys. Rev. Lett.* **83** 670-673 (1999) [arXiv:astro-ph/9901052].
- [3] C. L. Bennett *et al*, “First year *Wilkinson Microwave Anisotropy Probe* (WMAP) observations: Preliminary maps and basic results,” *Astrophys. J. Suppl.* **148** 1 (2003) [arXiv:astro-ph/0302207].
- [4] G. Hinshaw *et al*, “First year *Wilkinson Microwave Anisotropy Probe* (WMAP) observations: The angular power spectrum,” [arXiv:astro-ph/0302217].
- [5] R. R. Caldwell, M. Kamionkowski and N. N. Weinberg, “Phantom Energy and Cosmic Doomsday,” *Phys. Rev. Lett.* **91** 071301 (2003) [arXiv:astro-ph/0302506].
- [6] Z. Guo, Y. Piao, X. Zhang and Y. Zhang, “Cosmological evolution of a quintom model of dark energy,” *Phys. Lett. B* **608** 177-182 (2005) [arXiv:astro-ph/0410654].
- [7] X.F. Zhang, H. Li, Y. Piao Z. and X. Zhang, “Two-field models of dark energy with equation of state across -1 ,” [arXiv:astro-ph/0501652].
- [8] L. Perivolaropoulos, “Constraints on linear-negative potentials in quintessence and phantom models from recent supernova data,” *Phys. Rev. D* **71** 063503 (2005), [arXiv:astro-ph/0412308].
- [9] H. Wei and R. G. Cai, “Hessence: A New View of Quintom Dark Energy,” [arXiv:hep-th/0501160].
- [10] M. Li, B. Feng and X. Zhang, “A Single Scalar Field Model of Dark Energy with Equation of State Crossing -1 ,” [arXiv:hep-ph/0503268].
- [11] H. Stefancic, “Dark energy transition between quintessence and phantom regimes - an equation of state analysis,” [arXiv:astro-ph/0504518].
- [12] L. Perivolaropoulos, “Reconstruction of Extended Quintessence Potentials from the SNIa Gold Dataset,” [arXiv:astro-ph/0504582].
- [13] B. Feng, X. Wang and X. Zhang, “Dark Energy Constraints from the Cosmic Age and Supernova,” *Phys. Lett. B* **607** 35-41 (2005) [arXiv:astro-ph/0404224].
- [14] A. Vikman, “Can dark energy evolve to the Phantom?” *Phys. Rev. D* **71** 023515 (2005) [arXiv:astro-ph/0407107].
- [15] S. Nojiri, S. D. Odintsov and S. Tsujikawa, “Properties of singularities in (phantom) dark energy universe,” *Phys. Rev. D* **71**, 063004 (2005) [arXiv:hep-th/0501025].
- [16] B. Gumjudpai, T. Naskar, M. Sami and S. Tsujikawa, “Coupled dark energy: Towards a general description of the dynamics,” [arXiv:hep-th/0502191].
- [17] A. G. Riess *et al*, “Type Ia Supernova Discoveries at $z > 1$ From the Hubble Space Telescope: Evidence for Past Deceleration and Constraints on Dark Energy Evolution,” *Astrophys. J.* **607** 665-687 (2004), [arXiv:astro-ph/0402512].
- [18] M. Morris and K.S. Thorne, “Wormholes in spacetime and their use for interstellar travel: A tool for teaching General Relativity,” *Am. J. Phys.* **56**, 395 (1988).
- [19] M. S. Morris, K. S. Thorne and U. Yurtsever, “Wormholes, Time Machines and the Weak Energy Condition,” *Phys. Rev. Lett.* **61**, 1446 (1988).
- [20] Visser M 1995 *Lorentzian Wormholes: From Einstein to Hawking* (American Institute of Physics, New York)
- [21] S. Sushkov, “Wormholes supported by a phantom energy,” *Phys. Rev. D* **71**, 043520 (2005) [arXiv:gr-qc/0502084].
- [22] F. S. N. Lobo, “Phantom energy traversable wormholes,” *Phys. Rev. D* **71**, 084011 (2005) [arXiv:gr-qc/0502099].
- [23] M. Visser, S. Kar and N. Dadhich, “Traversable wormholes with arbitrarily small energy condition violations,” *Phys. Rev. Lett.* **90**, 201102 (2003) [arXiv:gr-qc/0301003].
- [24] S. Kar, N. Dadhich and M. Visser, “Quantifying energy condition violations in traversable wormholes,” *Pramana* **63**, 859-864 (2004) [arXiv:gr-qc/0405103].
- [25] C. Armendariz-Picon, “On a class of stable, traversable Lorentzian wormholes in classical general relativity,” *Phys. Rev. D* **65** (2002) 104010 [arXiv:gr-qc/0201027].
- [26] F. S. N. Lobo, “Surface stresses on a thin shell surrounding a traversable wormhole,” *Class. Quant. Grav.* **21** 4811 (2004) [arXiv:gr-qc/0409018].
- [27] J. P. S. Lemos, F. S. N. Lobo and S. Q. de Oliveira, “Morris-Thorne wormholes with a cosmological constant,” *Phys. Rev. D* **68**, 064004 (2003) [arXiv:gr-qc/0302049].
- [28] F. S. N. Lobo, “Energy conditions, traversable wormholes and dust shells,” [arXiv:gr-qc/0410087].
- [29] J. P. S. Lemos and F. S. N. Lobo, “Plane symmetric traversable wormholes in an anti-de Sitter background,” *Phys. Rev. D* **69** (2004) 104007 [arXiv:gr-qc/0402099].
- [30] E. Poisson and M. Visser, “Thin-shell wormholes: Linearization stability,” *Phys. Rev. D* **52** 7318 (1995) [arXiv:gr-qc/9506083].
- [31] E. F. Eiroa and G. E. Romero, “Linearized stability of charged thin-shell wormholes,” *Gen. Rel. Grav.* **36**, 651 (2004), [arXiv:gr-qc/0303093].
- [32] F. S. N. Lobo and P. Crawford, “Linearized stability analysis of thin-shell wormholes with a cosmological constant,” *Class. Quant. Grav.* **21**, 391 (2004) [arXiv:gr-qc/0311002].
- [33] M. Ishak and K. Lake, “Stability of transparent spherically symmetric thin shells and wormholes,” *Phys. Rev. D* **65** 044011 (2002).
- [34] G. Darrois, “Mémorial des sciences mathématiques XXV,” *Fascicule XXV ch V* (Gauthier-Villars, Paris, France, 1927).
- [35] W. Israel, “Singular hypersurfaces and thin shells in general relativity,” *Nuovo Cimento* **44B**, 1 (1966); and corrections in *ibid.* **48B**, 463 (1966).
- [36] P. F. González-Díaz, “Wormholes and ringholes in a dark-energy universe,” *Phys. Rev. D* **68**, 084016 (2003) [arXiv:astro-ph/0308382].
- [37] P. F. González-Díaz, “Achronal cosmic future,” *Phys. Rev. Lett.* **93** 071301 (2004) [arXiv:astro-ph/0404045].
- [38] V. Faraoni and W. Israel, “Dark energy, wormholes, and the Big Rip,” *Phys. Rev. D* **71** 064017 (2005), [arXiv:gr-qc/0503005].